BIOCHEMISTRY
including biophysical chemistry & molecular biology

Article

pubs.acs.org/biochemistry

A Transporter Motor Taken Apart: Flexibility in the Nucleotide Binding Domains of a Heterodimeric ABC Exporter

Magdalena A. Bukowska,[†] Michael Hohl,[†,‡] Eric R. Geertsma,[†,§] Lea M. Hürlimann,[†,‡] Markus G. Grütter,*[,†] and Markus A. Seeger*[,†,‡]

[†]Department of Biochemistry, University of Zurich, Winterthurerstrasse 190, 8057 Zurich, Switzerland

[‡]Institute of Medical Microbiology, University of Zurich, Gloriastrasse 30/32, 8006 Zurich, Switzerland

Supporting Information

ABSTRACT: ABC exporters are ubiquitous multidomain transport proteins that couple ATP hydrolysis at a pair of nucleotide binding domains to substrate transport across the lipid bilayer mediated by two transmembrane domains. Recently, the crystal structure of the heterodimeric ABC exporter TM287/288 was determined. One of its asymmetric ATP binding sites is called the degenerate site; it binds nucleotides tightly but is impaired in terms of ATP hydrolysis. Here we report the crystal structures of both isolated motor domains of TM287/288. Unexpectedly, structural elements constituting the degenerate ATP binding site are disordered in these crystals and become structured only in the context of the full-length transporter. In addition, hydrogen bonding patterns of key residues, including those of the catalytically important Walker B and the switch loop motifs, are fundamentally different in the solitary NBDs compared to those in the intact transport protein. The structures reveal crucial interdomain contacts that need to be established for the proper assembly of the functional transporter complex.

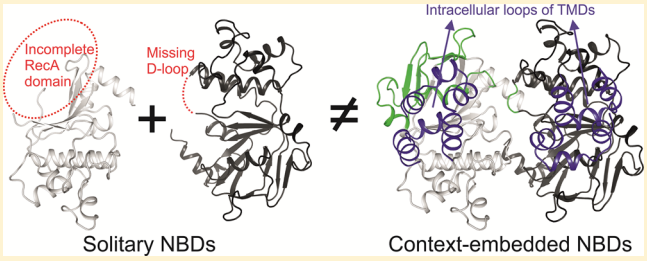

ATP binding cassette (ABC) transporters constitute one of the largest membrane protein families and are abundantly represented in all kingdoms of life. These multidomain integral membrane proteins utilize the energy of ATP hydrolysis to drive translocation of various compounds across cellular membranes. ABC transporters are crucial for physiological processes as diverse as the uptake of nutrients, homeostasis maintenance, resistance to toxins, or antigen processing.[1] When impaired, the ABC transporters can cause hereditary diseases in humans, including cystic fibrosis,[2] Stargardt disease,[3] and adrenoleukodystrophy.[4] In addition, ABC transporters are notorious for causing multidrug resistance in tumor cells.[5]

All ABC transporters share a canonical architecture comprising two transmembrane domains (TMDs) and two cytosolic nucleotide binding domains (NBDs). The fold of the ATP binding cassette has been established by numerous previously reported structures of isolated NBDs (more than 50 NBD structures are listed in ref 6) and full-length ABC transporters.[7−19] NBDs are divided into two major parts, the RecA-like domain and the helical domain. The RecA-like domain consists of two β-sheets, sheet 1 and sheet 2.[20,21] The RecA-like domain harbors the Walker A motif, which interacts with the β- and γ-phosphates of bound nucleotides, the Walker B motif, which contains a catalytic glutamate, the H-loop (also called switch loop) with a conserved histidine, the D-loop with a conserved aspartate, and the A-loop with a conserved aromatic residue required for π-stacking interactions with the adenine ring of ATP. The helical domain is a bundle of α-helices typical for ABC transporters and contains the ABC signature motif that contacts the γ-phosphate of the ATP in a closed NBD dimer.[22−24] The functional NBD dimer contains two composite ATPase sites with both NBDs contributing to each of them. The Walker A motif, Walker B motif, and the H-loop of one NBD are complemented with the signature motif of the second NBD so that nucleotides become sandwiched between the two NBDs. Many heterodimeric ABC exporters, including the medically relevant examples TAP1/2, CFTR, and SUR1, exhibit an intriguing asymmetry of the NBDs.[25−27] Typically, NBD1 has an aspartate in place of a conserved glutamate in the Walker B motif, and the histidine of the H-loop is substituted with a glutamine. NBD2 has a noncanonical signature motif. Upon NBD heterodimerization, the divergent motifs align to form a noncanonical ATPase site, while the other site consists of consensus motifs. The consensus site has been demonstrated to be largely or solely responsible for ATPase activity and for NBD closure.[28] In contrast, the noncanonical site is suggested to be catalytically impaired.

Until recently, structural information about heterodimerized NBDs displaying nonequivalent ATP binding sites was lacking. It was the high-resolution structure of full-length TM287/288, a heterodimeric ABC exporter from *Thermotoga maritima*, that permitted first insights into a heterodimeric NBD interface.[29]

Received: February 24, 2015
Revised: April 21, 2015
Published: May 7, 2015

DOI: 10.1021/acs.biochem.5b00188
Biochemistry 2015, 54, 3086−3099

The transporter was crystallized in its inward-facing conformation, and the structure revealed that the NBDs are only partially disengaged even in the absence of nucleotides.[30] So far, all ABC exporters crystallized in an inward-facing conformation showed a separation of the NBDs with varying distances between them.[8,9,15−18,31] Although distantly spaced NBDs were confirmed by EPR spectroscopy,[32,33] other studies casted doubts on whether the large NBD separation is necessary for drug transport.[34] Surprisingly, there are no examples of ABC exporters for which the NBDs have been described in the full-length context and as solitary domains. By contrast, the NBDs of the maltose transporter, a well-characterized type I ABC importer, have been crystallized both in isolation and in the context of the full-length transporter complex.[10,35]

If one aims to understand a transport machine in detail, one has to study its individual parts, as well. Therefore, we expressed, purified, crystallized, and biochemically characterized the isolated motor domains, the NBDs, of TM287/288. The isolated halves of the motor were in part unstructured and deficient in ATP hydrolysis. A comparison of the presented nucleotide-free structures with the identical domains embedded in full-length apo TM287/288[30] highlights interdomain contacts, which are critical for the proper assembly and functioning of the transport machinery.

MATERIALS AND METHODS

Generation of the Expression Constructs. FX cloning vectors for expression of proteins with noncleavable Avi tags (detailed in Table S1 of the Supporting Information) were constructed by polymerase chain reaction (PCR) using pBXC3GH, pBXC3H, or pBXNH3 as a template.[36] DNA sequences encoding N- and C-terminal Avi tags in pBXC3H and pBXC3GH were introduced using primer set 1 (5′-CTC AGA AAA TCG AAT GGC ACG AAA GTT GAA GAG CGA CCT GCA GAC TG and 5′-CTT CGA AGA TAT CGT TCA GAC CAG CCA TGG TTA ATT CCT CCT GTT AGC CC) and primer set 2 (5′-CTC AGA AAA TCG AAT GGC ACG AAT TAG AAG TTT TGT TTC AAG GTC CAC A and 5′-CTT CGA AGA TAT CGT TCA GAC CTG CAG AAG AGC AAA ACT AGT GGA TC), respectively. DNA sequences encoding N- and C-terminal Avi tags in pBXNH3 were introduced using primer set 3 (5′-CTC AGA AAA TCG AAT GGC ACG AAA GTT GAA GAG CGA CCT GCA GAC TG and 5′-CTT CGA AGA TAT CGT TCA GAC CTG GAC CTT GAA ACA AAA CTT CTA AAT G) and primer set 4 (5′-CTT CGA AGA TAT CGT TCA GAC CTG CAG AAG AGC AAA ACT AGT GGA TC and 5′-CTC AGA AAA TCG AAT GGC ACG AAT AAT AAC TAG AAC AAA AAC TCA TCT CAG AAG), respectively. Plasmids were amplified by PCR using the Phusion DNA polymerase, and the template was subsequently digested with DpnI. The gel-purified PCR product was supplemented with polynucleotide kinase buffer, incubated for 10 min at 70 °C, and placed on ice. Subsequently, 1 mM ATP and 1 unit/μL polynucleotide kinase (final concentrations) were added, and the sample was incubated for 60 min at 37 °C. After the addition of fresh ATP and T4 ligase (final concentrations of 1 mM and 0.1 unit/μL, respectively) the sample was incubated for 60 min at 25 °C and for 20 min at 65 °C, subsequently transformed into *Escherichia coli* DB3.1 cells,[37] and plated on LB agar plates supplemented with ampicillin and chloramphenicol (final concentrations of 100 and 34 μg/mL, respectively). Relevant regions of the plasmids were verified by sequencing. Vector pETM11-SUMO3GFP[38] was used as the only pET-based vector for test expressions. For this purpose, the vector was modified to make it amenable for FX cloning. An undesirable SapI site on pETM11-SUMO3GFP was removed by QuikChange mutagenesis using the primers pETM11_SUMO_delSapI_for (5′-GAG GAA GCG GAT GAG CGC CTG-3′) and pETM11_SUMO_delSapI_rev (5′-CAG GCG CTC ATC CGC TTC CTC-3′). This SapI-free pETM11-SUMO3GFP vector was then cleaved with the restriction enzymes AgeI and HindIII and ligated with the two annealed oligonucleotides, pETM11_FX_for (5′-CCG GTG GAA GTA GAA GAG CAT ATG CTC TTC TGC ATA ATA-3′) and pETM11_FX_rev (5′-AGC TTA TTA TGC AGA AGA GCA TAT GCT CTT CTA CTT CCA-3′), which encode the two required SapI restriction sites and form overhangs compatible with cloning into AgeI and HindIII. The ccdB kill cassette and a chloramphenicol resistance marker were excised from pBXNH3 by SapI and ligated into the SapI-digested pETM11-SUMO_FX vector.

Cloning of the NBDs into the Expression Vectors. The two NBDs of the heterodimeric ABC transporter TM287/288 were amplified from vector pBXNH3_TM287/288 used for the determination of the structure of the full-length transporter.[29] Each NBD was cloned into 10 different *E. coli* expression vectors using the FX cloning method.[36] The primers NBD287_for (5′-ATA TGC TCT TCT AGT GGG AGC GTT TCC TTC GAA AAT GTC-3′), NBD287_rev (5′-TAT AGC TCT TCA TGC GGC ATC GTT CAT CAC CCC GTT TCC-3′), NBD288_for (5′-ATA TGC TCT TCT AGT GGA GAA ATC GAG TTC AAG AAT GTC-3′), and NBD288_rev (5′-TAT AGC TCT TCA TGC TGC TTC TTT TTC TAC AAC GAG ACC-3′) were used to amplify the two soluble domains, both starting with a conserved glycine residue [Gly330 (NBD287) and Gly353 (NBD288) of the full-length transporter]. The inserts were cloned into the FX expression vectors pBXNH3, pBXC3H, pBXC3GH,[36] and pETM11-SUMO_FX. Additionally, both inserts were ligated into Avi tag vectors pBXNH3A, pBXNH3CA, pBXNAC3H, pBXNAC3GH, pBXCA3H, and pBXCA3GH. Table S1 of the Supporting Information illustrates the nomenclature used for the vector annotation.

Test Expression of NBD287 and NBD288. *E. coli* MC1061 (for pBX vectors) and BL21(DE3) cells (for pET vectors) transformed with the corresponding vectors were used to produce the NBDs in shaking flasks containing 100 mL of LB medium, 100 μg/mL ampicillin (pBX), or 50 μg/mL kanamycin (pET) at 30 °C. Protein production was induced with 0.0025% L-arabinose (pBX) or 0.5 mM isopropyl β-D-1-thiogalactopyranoside (IPTG) (pET) at an OD_{600} of 1 for ∼4 h. The cells were then spun down at 5000*g* and frozen at −20 °C. After resuspension in 20 mM Tris-HCl (pH 8.0), 200 mM NaCl, and 3 mM $MgCl_2$ and addition of DNase I, the cells were disrupted by sonication. Cell debris were removed by centrifugation (SS34 rotor, 15000*g*, 30 min). The supernatant was subsequently loaded onto a Ni^{2+}-NTA column and washed with 50 mM imidazole (pH 7.5), 200 mM NaCl, and 10% glycerol. The protein was eluted using the same buffer containing 200 mM imidazole (pH 7.5). Collected fractions were analyzed for expression yield via sodium dodecyl sulfate−polyacrylamide gel electrophoresis (SDS−PAGE). The best expressing constructs were further analyzed by SEC using a Superdex 75 10/300 GL column.

DOI: 10.1021/acs.biochem.5b00188
Biochemistry 2015, 54, 3086−3099

Expression and Purification of NBD287. If not stated otherwise, all purification steps were performed at 4 °C. NBD287 was expressed using the pETM11-SUMO_FX_NBD287 construct, which adds a cleavable His_6-SUMO fusion to the N-terminus of NBD287. Freshly transformed *E. coli* BL21(DE3) cells were cultured in LB medium at 37 °C in the presence of kanamycin (50 μg/mL) until the OD_{600} reached 0.8. The culture was then induced by IPTG (final concentration of 0.1 mM), and expression was conducted for 4 h at 30 °C. For cell lysis, the pellet was resuspended in lysis buffer [20 mM Tris-HCl (pH 8.0), 200 mM NaCl, 10 mM imidazole (pH 7.5), 2 mM $MgCl_2$, EDTA-free protease inhibitor cocktail (Roche), 1 mM PMSF, and 10 μg/mL DNase I]. Upon disruption, the lysate was cleared by centrifugation (SS34 rotor, 20000 rpm, 30 min) and applied to a gravity flow Ni^{2+}-NTA column equilibrated with 20 mM Tris-HCl (pH 8.0), 200 mM NaCl, 10 mM imidazole (pH 7.5), and 10% glycerol. The resin was washed with 30 mL of the same buffer containing 40 mM imidazole (pH 7.5), and the SUMO-NBD287 fusion was eluted in the buffer containing 200 mM imidazole (pH 7.5). For buffer exchange into 20 mM Tris-HCl (pH 7.5) and 150 mM NaCl, the protein was applied onto a PD-10 desalting column (GE Healthcare) prior to an overnight proteolytic cleavage of the SUMO tag using the SenP2 protease [at a 1:500 (w/w) SenP2:SUMO3-NBD287 fusion ratio]. SUMO and SenP2, both still containing His tags, were removed by Ni^{2+}-NTA chromatography. Directly prior to crystallization, cleaved NBD287 was subjected to SEC (Superdex 75 10/300 GL) with 20 mM Tris-HCl (pH 7.5) and 150 mM NaCl (SEC buffer). The peak corresponding to the NBD287 monomer was concentrated to ∼12 mg/mL.

Expression and Purification of NBD288-Avi and NBD288. NBD288 used in this study was expressed in expression vector pBXCA3GH or pBXC3H (Table S1 of the Supporting Information). For protein overexpression, freshly transformed *E. coli* MC1061 cells were grown in 2YT medium supplemented with ampicillin (100 μg/mL) to an OD_{600} of 1 and were then induced by adding L-arabinose [final concentration of 0.0025% (w/v)]. The expression was conducted for 5 h at 30 °C. Cells were disrupted and the proteins purified by Ni^{2+}-NTA chromatography as described above for NBD287. Despite the addition of DNase I prior to cell lysis, we consistently observed large amounts of contaminating DNA, which was copurified with NBD288 during Ni^{2+}-NTA chromatography as judged from A_{260}/A_{280} ratios of >1.5. To remove DNA, the Ni^{2+}-NTA eluate was treated with 2 mM $MgCl_2$ and 25 μg/mL DNaseI at room temperature for 30 min, and the sample was diluted with buffer to reduce the imidazole concentration to 25 mM and repurified by Ni^{2+}-NTA chromatography. The GFP-His tag (pBXCA3GH) and the His tag (pBXC3H) were removed by an overnight enzymatic cleavage using a His-tagged 3C protease at a 1:20 (w/w) ratio of enzyme to fusion protein. The cleaved tags and the protease were rebound to the Ni^{2+}-NTA agarose to obtain pure NBD288-Avi or NBD288. Directly before crystallization, NBD288-Avi or NBD288 was subjected to SEC (Superdex 75 10/300 GL) and concentrated to ∼10 mg/mL.

Analytical SEC. Analytical SEC shown in Figure 1 was performed using a Superdex 200 5/150 GL column. The SEC analysis shown in Figure S1 of the Supporting Information was performed using a Superdex 75 10/300 GL column. For the runs without nucleotides, the column was equilibrated with SEC buffer and samples were incubated with 1 mM EDTA to exclude potential effects caused by any contaminating magnesium. For the analysis in the presence of ATP, the column was equilibrated with SEC buffer containing 1 mM $MgCl_2$ and 1 mM ATP and the protein samples were incubated with 1 mM MgATP prior to injection. The NBD mixture was prepared by mixing equimolar amounts of NBD domains.

ATPase Measurements. ATPase assays of purified NBD287, NBD288, and TM287/288 were performed in SEC buffer containing 10 mM $MgSO_4$ and 0.03% β-DDM for all measurements. The assay was conducted at 30 or 50 °C for 30 min in the presence of 5 mM ATP. The protein concentrations were 2 μM for NBD287 and NBD288 and 4 or 1 nM for TM287/288 for the measurements at 30 or 50 °C, respectively. Liberated P_i was determined by malachite green detection as described in ref 30.

Scintillation Proximity Assay (SPA). The SPA was performed as previously described for TM287/288.[29] Purified NBD287 (as a His_6-SUMO-NBD fusion), NBD288, NBD288_Y364A, and NBD288_K394M (as NBD-3C-His_{10} fusions) and TM287/288 (containing an N-terminal His_{10} tag on TM287) were immobilized at a final concentration of 200 nM on PVT copper His-tag SPA beads (PerkinElmer, 2 mg/mL) in 20 mM Tris-HCl (pH 7.5), 150 mM NaCl, and 3 mM $MgCl_2$ supplemented with 0.03% β-DDM for full-length TM287/288. The preloaded beads (140 μL/well) were aliquoted in a white-framed isoplate-96 (PerkinElmer). [^{3}H]ATP (1 mCi/mL, PerkinElmer) and [^{3}H]ADP (1 mCi/mL, Hartmann Analytics) were mixed with cold nucleotides and added at final concentrations of 5, 10, 20, 50, 100, and 200 μM with final volumetric activities of 1.875, 3.75, 7.5, 15, 24, and 23 μCi/mL, respectively, to each well. The plates were incubated overnight on an orbital microplate shaker at 4 °C and then counted on a PerkinElmer 1450-028 Trilux MicroBeta counter (SPA cpm mode). In the case of measurements with [^{3}H]ATP, 200 nM GFP (as GFP-3C-His_{10} fusion) was immobilized on SPA beads for background subtraction, because the background levels of empty beads were slightly higher than those of NBD287 and the NBD288 mutants, resulting in negative binding values. We reasoned that this problem originated from ionic interactions between strongly negatively charged ATP and the positively charged copper-coated SPA beads, which become weaker if GFP is bound via its His_{10} tag to the beads. For the measurements with [^{3}H]ADP, the problem did not occur and empty beads served for background subtraction. Importantly, unambiguous [^{3}H]ATP binding was observed for NBD288 and TM287/288 regardless whether GFP-loaded beads or empty beads served for background subtraction. The curves for binding of [^{3}H]ATP to TM287/288 and NBD288 were not fit because TM287/288 has two asymmetric binding sites that would require more data points to allow for fitting with a two-site saturation curve (as shown in ref 29), and because for NBD288 the binding signal was not saturated at 200 μM [^{3}H]ATP. Higher [^{3}H]ATP concentrations could not be sampled because above 200 μM, cold ATP competed for binding of hot ATP too strongly, resulting in small differences between NBD288 samples and background.

Unfolding Using the Fluorescent Reporter Dye SYPRO Orange. Thermal unfolding of NBD287, NBD288, and TM287/288 was performed in a 20 μL reaction volume containing 50 mM Na-HEPES (pH 7.5), 150 mM NaCl, and 112× SYPRO Orange (Life Technologies). The protein concentrations were as follows: 3.25 μM NBD287, 3 μM

DOI: 10.1021/acs.biochem.5b00188
Biochemistry 2015, 54, 3086−3099

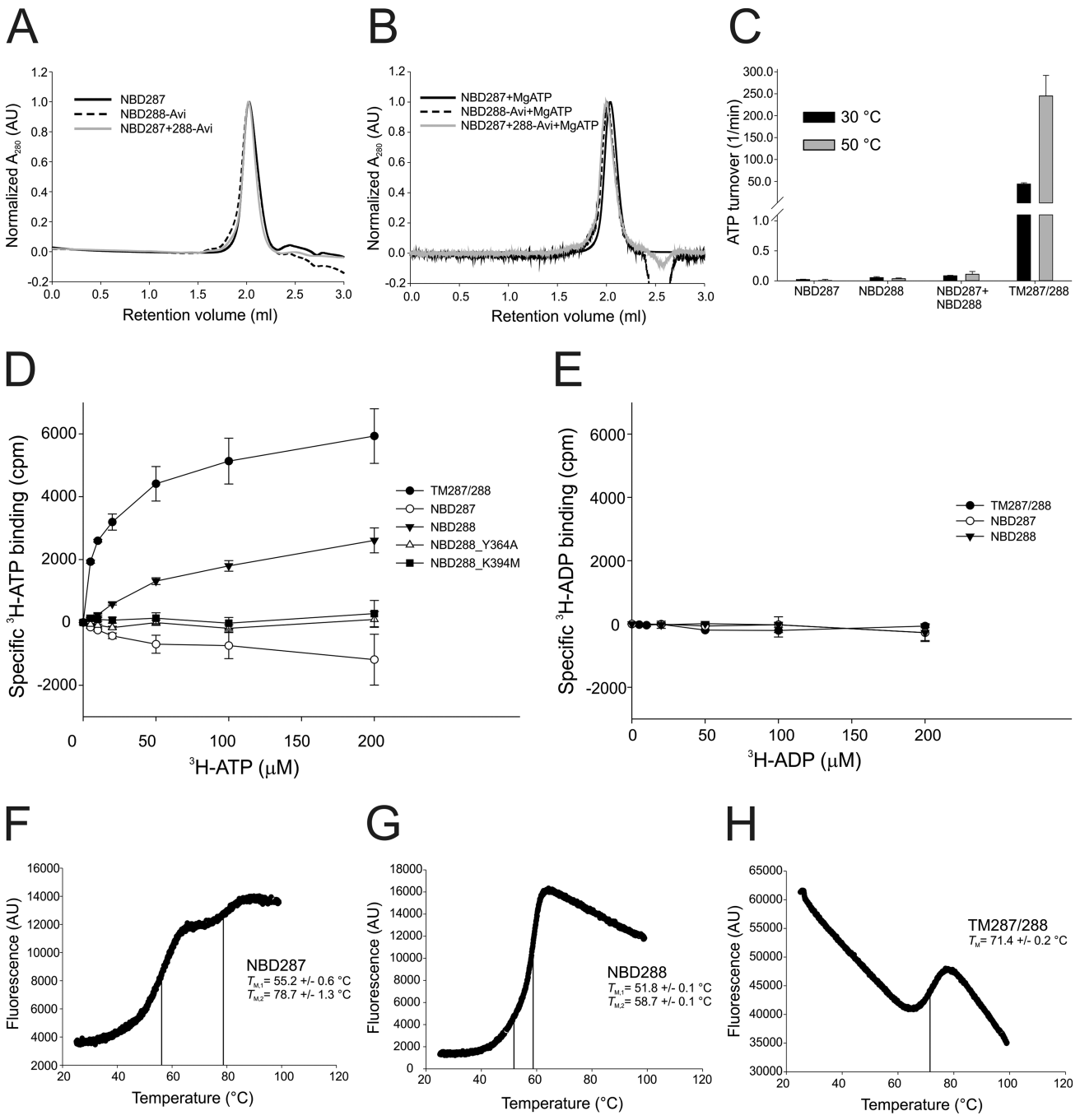

Figure 1. Biochemical analysis of the NBDs. Analytical SEC of the NBDs using a Superdex 200 5/150 column in the absence of nucleotides (A) and in the presence of 1 mM MgATP (B). (C) ATPase activities of the NBDs and full-length TM287/288 determined in the presence of 5 mM MgATP. The activities were calculated as ATP turnover of each protein molecule per minute. Error bars correspond to standard deviations based on quadruplicates. Binding of [^{3}H]ATP (D) and [^{3}H]ADP (E) to the NBDs and full-length TM287/288 determined by a scintillation proximity assay. NBD288 mutants NBD288_Y364A and NBD288_K394M served as controls. Error bars correspond to standard deviations calculated from duplicates. Thermal unfolding of NBD287 (F), NBD288 (G), and TM287/288 (H) monitored using SYPRO Orange. The midpoints of transitions (T_Ms) were obtained by fitting the first derivative of the fluorescent signal to Gaussian equations (see Figure S2 of the Supporting Information). Statistical errors correspond to standard deviations based on triplicates.

NBD288, and 1.2 μM TM287/288. The fluorescent signal of SYPRO Orange was followed in a 7500 Fast Real-Time PCR System (Life Technologies) using filter 4 (ROX) and by performing a temperature ramp from 25 to 99 °C over a time frame of 75 min. Curves of samples containing buffer instead of protein were measured and used for background subtraction. The data were exported to Excel; the background was subtracted, and the first derivative was determined and fit to the "Sum of two Gaussians" equation in GraphPad Prism that is defined as follows:

$$y_1 = \text{amplitude}_1 \times \exp\{-0.5[(x - \text{mean}_1)/\text{SD}_1]^2\}$$

$$y_2 = \text{amplitude}_2 \times \exp\{-0.5[(x - \text{mean}_2)/\text{SD}_2]^2\}$$

$$y = y_1 + y_2$$

DOI: 10.1021/acs.biochem.5b00188
Biochemistry 2015, 54, 3086−3099

Here, $mean_1$ and $mean_2$ correspond to the midpoints of transition $T_{M,1}$ and $T_{M,2}$, respectively.

The data of TM287/288 were fit to a single Gaussian equation:

$$y = \text{amplitude}_1 \times \exp\{-0.5[(x - \text{mean})/\text{SD}_1]^2\}$$

in which mean corresponds to T_M. The first derivatives and the Gaussian fits are shown in Figure S2 of the Supporting Information.

Crystallization and Structure Determination. The samples of NBD287, NBD288-Avi, and NBD288 were subjected to vapor diffusion crystallization performed at 20 °C. Initial crystal hits of NBD287 were refined using hanging drops. The protein was mixed in a 1:1 ratio with reservoir solution containing 100 mM Tris-HCl (pH 7.8), 100 mM sodium acetate, and 25% (w/v) PEG2000 MME. The crystals were transferred into mother liquor solution containing 30% PEG2000 MME prior to being cryo-cooled in liquid nitrogen. Several conditions yielded crystals of NBD288-Avi, and the final data were collected from a crystal grown in sitting drops in a 1:1 mixture with the reservoir solution 100 mM sodium acetate (pH 5.5), 6% (w/v) PEG550 MME, 6% (w/v) PEG20000, and 200 mM $MgCl_2$. The crystals were transferred into mother liquor containing 25% ethylene glycol and frozen in liquid nitrogen. NBD288 yielded crystals under dozens of initial conditions, and the crystals were directly frozen from such a nanoliter sitting drop experiment without further cryo-protection. The structure was determined from a condition containing 100 mM Tris-HOAc (pH 7.5), 200 mM $MgCl_2$, 8% PEG550 MME, and 8% PEG20000. Diffraction data were collected at beamline X06SA of the Swiss Light Source (SLS, Villigen, Switzerland) equipped with a PILATUS detector (Dectris). Data were indexed with XDS[39] and scaled with XSCALE of the CCP4 package. The free R factor (R_{free}) was calculated from 5% of randomly chosen reflections. The phases were obtained by molecular replacement in PHASER[40] using models derived from the full-length TM287/288 transporter structure [Protein Data Bank (PDB) entry 3QF4]. The structure was built into the electron density using COOT[41] and refined with PHENIX.[42]

Cocrystallization and Soaking Attempts with Nucleotides. For NBD287 and NBD288, extensive cocrystallization trials with ATP, AMP-PNP, or ADP (2.5 mM each supplemented with 3 mM $MgCl_2$) were performed. However, cocrystallization attempts did not yield diffracting crystals different from those obtained in the absence of nucleotides. The crystals obtained for NBD287 (space group 179) and NBD288 (space group 145) were soaked with 2.5 mM ATP, AMP-PNP, or ATP in the presence of 3 mM $MgCl_2$. Data sets of the corresponding crystals were collected (diffraction in all cases better than 3 Å), but nucleotide binding was not observed.

Analysis of the Dissolved NBD287 Crystals. NBD287 crystals were washed four times in the reservoir solution and dissolved in SDS–PAGE loading buffer for analysis of its electrophoretic behavior or in distilled water for mass spectrometry. MALDI-MS analysis was performed at the Functional Genomics Center Zurich (FGCZ).

RESULTS

Protein Expression and Purification. The solitary NBDs of the heterodimeric ABC exporter TM287/288 were termed NBD287 and NBD288, and the same domains in the full-length context were named NBD1 and NBD2, respectively. NBD287 (residues 330–577) and NBD288 (residues 353–592) were each cloned into 10 different expression vectors using the FX cloning strategy,[36] adding a His tag and in addition Avi, GFP, or SUMO tags in various combinations to the N- or C-terminus of the expressed NBDs (Table S1 of the Supporting Information). Proteins were expressed in and purified from *E. coli* by Ni^{2+}-chelating chromatography, followed by tag cleavage and size exclusion chromatography (SEC). Only in a limited number of expression vectors used were NBD287 and NBD288 produced in sufficient amounts and as monodisperse proteins (Table S1 of the Supporting Information). NBD287 was produced using the pETM11-SUMO_FX construct containing a SUMO solubility tag at its N-terminus, which was cleaved by SenP2 protease after Ni^{2+}-chelating chromatography. NBD288 was produced from the pBXC3H construct containing a His_{10} tag fused to the C-terminus, which was cleaved by 3C protease. In addition, we also expressed NBD288 from vector pBXCA3GH, which adds a noncleavable Avi tag and a cleavable GFP tag to the C-terminus of the domain. The resulting protein was called NBD288-Avi.

Biochemical and Functional Characterization of Purified NBD287 and NBD288. Numerous NBDs stemming from homodimeric ABC exporters, including HlyB,[43] MJ0796,[44] and MsbA,[45] were shown to form dimers in the presence of nucleotides. Therefore, the oligomeric states of NBD287, NBD288, and NBD288-Avi were studied using SEC. This analysis suggests that the NBDs are monomers in solution and did not deliver any indication of ATP-induced dimerization, even if both NBDs were mixed for heterodimer formation (Figure 1A,B and Figure S1 of the Supporting Information). We reasoned that lack of dimerization in the presence of MgATP could be due to ATP hydrolysis, which initiates disengagement of the NBDs. However, the NBDs exhibited barely detectable ATPase activities at temperatures of 30 and 50 °C, 5 mM ATP, and NBD concentrations of 2 μM (ATP turnover of <0.1 min^{-1}), while the ATP turnover of the purified full-length transporter was 44 ± 3 min^{-1} (at 30 °C) and 244 ± 47 min^{-1} (at 50 °C) (Figure 1C). Mixing of the NBDs did not result in a marked increase in ATPase activity. Whereas the ATPase activity of full-length TM287/288 increased 5.6-fold when the temperature was shifted from 30 to 50 °C, the small ATPase activities of the isolated NBDs did not change. Next, we assessed in a scintillation proximity assay[29] whether the purified NBDs bind the tritium-labeled nucleotides ATP and ADP (Figure 1D,E). Full-length TM287/288 and isolated NBD288 were capable of binding ATP, but not ADP. NBD287 was deficient in binding nucleotides. To further investigate whether binding of ATP to NBD288 was specific, we individually mutated the A-loop tyrosine to alanine (NBD288_Y364A) and the Walker A lysine to methionine (NBD288_K394M). Both residues have been shown in other ABC transporters to be important for nucleotide binding[46,47] and resulted in a loss of binding of ATP to NBD288 (Figure 1D). Finally, we performed a temperature unfolding experiment with NBD287, NBD288, and full-length TM287/288 using SYPRO Orange as a fluorescent reporter dye, which binds to exposed core residues of denatured proteins (Figure 1F–H and Figure S2 of the Supporting Information).[48] Whereas the unfolding curves for NBD287 and NBD288 were biphasic with their main midpoints of transition at 55.2 ± 0.6 and 58.7 ± 0.6 °C, respectively, full-length TM287/288 exhibited a single

DOI: 10.1021/acs.biochem.5b00188
Biochemistry 2015, 54, 3086–3099

Table 1. Data Collection and Refinement Statistics

	NBD287 (PDB entry 4Q7K)	NBD288 (PDB entry 4Q7L)	NBD288-Avi (PDB entry 4Q7M)
		Data Collection[a]	
space group	$P6_522$ (179)	$P3_2$ (145)	$P3_221$ (154)
cell dimensions			
a (Å)	80.17	95.93	58.30
b (Å)	80.17	95.93	58.30
c (Å)	129.57	88.51	208.69
α (deg)	90.00	90.00	90.00
β (deg)	90.00	90.00	90.00
γ (deg)	120.00	120.00	120.00
resolution (Å)	100−1.8 (1.85−1.80)	50−2.35 (2.41−2.35)	100−2.3 (2.36−2.30)
R_{meas} (%)	5.0 (201.0)	8.8 (112.7)	9.4 (97.4)
I/σ_I	41.11 (2.27)	15.83 (2.86)	19.66 (3.31)
$CC_{1/2}$ (%)	99.9 (85.5)	99.8 (74.3)	99.6 (88.3)
completeness (%)	100 (100)	99.3 (99.2)	99.9 (100.0)
redundancy	38.1 (37.1)	5.1 (5.2)	11.6 (12.4)
		Refinement	
resolution (Å)	50−1.8	50−2.35	100−2.3
no. of reflections (work/test)	23505/1175	37661/1885	19132/957
R_{work}/R_{free} (%)	20.42/21.15	19.31/23.63	18.06/23.60
no. of atoms			
protein	1463	5950	2036
water	61	218	128
total *B* factor (Å^2)	61.5	56.3	48.3
root-mean-square deviation			
bond lengths (Å)	0.007	0.004	0.006
bond angles (deg)	1.126	0.853	0.944

[a]Values in parentheses are for the last resolution shell.

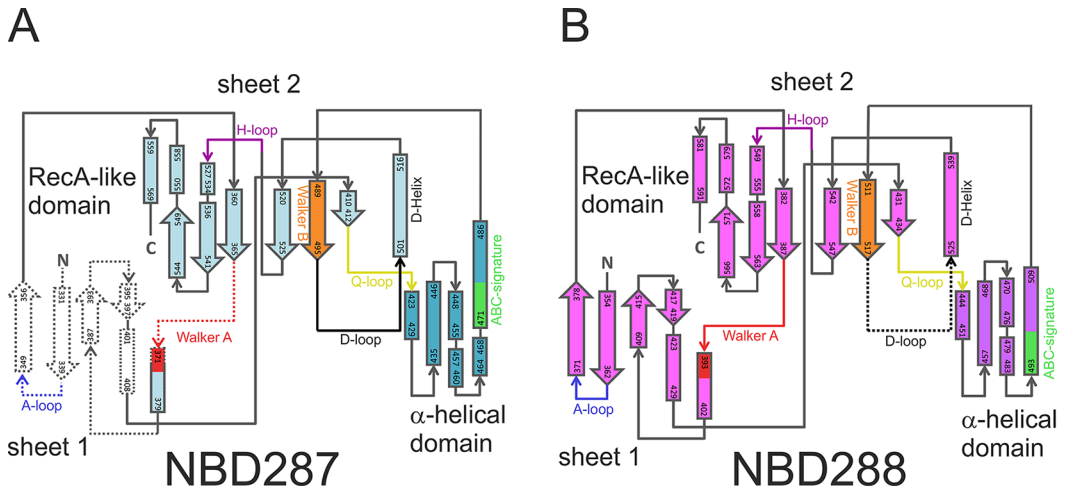

Figure 2. Topology schemes of the NBDs indicating subdomain organization and position of the conserved elements. The A-loop is colored blue, the Walker A motif red, the Walker B motif orange, the H-loop purple, the ABC signature motif green, the Q-loop yellow, and the D-loop black. Dotted lines indicate areas not resolved in the structures. (A) NBD287 and (B) NBD288.

midpoint of unfolding at 71.4 ± 0.6 °C. This analysis indicated that (i) the isolated domains are considerably less stable than the full-length transporter and (ii) NBD287 and NBD288 were nevertheless sufficiently stable to warrant protein integrity in the biochemical analyses performed. In summary, despite the fact that we had stable and monodisperse NBDs in our hands, we observed a lack of nucleotide binding (for NBD287) and a lack of ATPase activity (for both NBDs) under experimental conditions that permit ATP binding and hydrolysis by the full-length transporter. To obtain a structural rationale for this lack of function, NBD287, NBD288, and NBD288-Avi were crystallized.

Structural Analysis of NBD287. Crystals of NBD287 diffracted to 1.8 Å resolution, and the structure was determined by molecular replacement using NBD1 of the TM287/288 structure as a search model (Table 1). The final model includes residues 353−366, 373−382, and 407−570, which encompasses the helical domain and sheet 2 of the RecA-like domain but lacks sheet 1 of the RecA-like domain, the loop containing the Walker A motif and seven C-terminal residues (Figure 2A). The other functionally relevant motifs, including the ABC

DOI: 10.1021/acs.biochem.5b00188
Biochemistry 2015, 54, 3086−3099

signature, Walker B, D-loop, and switch motifs, are well-ordered.

Residues 373−382 fold as a helix immediately following the Walker A motif in the full-length transporter. In NBD287, the same residues form an amphipathic helix, which binds via a hydrophobic patch into a groove formed by the β-sheets of sheet 2 (Figure S3A of the Supporting Information). The structural arrangement of this Walker A helix in isolated NBD287 is completely different from that observed in the full-length context (Figure S3B of the Supporting Information) and other structures of isolated NBDs and is therefore physiologically most likely irrelevant. Because NBD287 elutes as monomer from SEC (Figure 1A), the structure suggests that isolated NBD287 has been crystallized in a partially structured, stable folding intermediate. However, the possibility that crystallization artifacts are the cause of missing density in sheet 1 cannot be ruled out. Analysis of dissolved NBD287 crystals by SDS−PAGE and mass spectrometry did not reveal protein fragmentation (Figure S4 of the Supporting Information), excluding the possibility that NBD287 was proteolytically cleaved. For clarity of discussion, residues 373−382 were omitted from the structural analysis of NBD287. A functional head-to-tail dimer of NBD287 molecules was not observed in the crystal.

Superposition of the structured part of NBD287 in isolation with its counterpart of the full-length TM287/288 apo structure (PDB entry 4Q4H) results in a root-mean-square deviation (rmsd) of 1.542 Å calculated over 173 Cα atoms. When only the RecA-like domain is used for superposition, a rotation of the helical domain becomes apparent. In the isolated domain, the bundle of helices rotates away from the core β sheet by 12° relative to the TM287/288 structure (Figure 3A). This flexible hinge between the RecA-like domain and the helical domain has been described for numerous isolated NBDs,[6,28,49,50] and the inward rotation had been associated with nucleotide binding.[24,51]

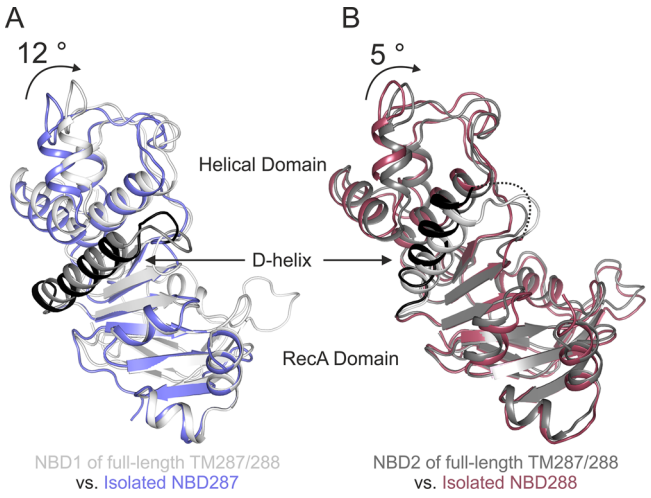

Figure 3. Rigid body rotations of NBDs in isolation and in the full-length transporter context. The RecA-like domains of NBD287 (A) and NBD288-chainC (B) were superimposed on full-length apo TM287/288. (A) A rigid body rotation of 12° is required to superimpose the helical domain of isolated NBD287 (blue) on that in TM287/288 (light gray). The D-loop and D-helix are colored black (NBD287) and light gray (TM287/288). (B) A rigid body rotation of 5° is observed between the helical domains of NBD288-chainC (raspberry) and TM287/288 (dark gray). An outward rotation of the D-helix of NBD288-chainC (black) is seen relative to the corresponding D-helix in TM287/288. The missing D-loop of NBD288-chainC is indicated by a dashed line.

Hydrogen Bonding Pattern of Isolated NBD287 in Comparison to the Domain Embedded in Full-Length TM287/288. We compared the hydrogen bonding patterns mediated by conserved residues in the isolated domain and in the context of full-length TM287/288 (Figure 4A,B and Figure S5 of the Supporting Information). In isolation, the non-canonical Walker B Asp495 points toward the switch loop and makes a hydrogen bond (threshold of ≤3.6 Å) with Gln526 that substitutes the canonical histidine of the catalytic dyad, while the Q-loop Gln414 interacts with the D-loop Ser498 (Figure 4A). In full-length TM287/288, the carboxyl side chain of Asp495 is within hydrogen bonding distance of Gln414 and Gln526 interacts with residues of the D-loop of the opposite NBD2 (Figure 4B). Thus, there are major differences in the hydrogen bonding pattern between NBD287 in isolation and the same domain embedded in the full-length structure in which conserved key residues interact with NBD2.

Structures of Isolated NBD288. Two NBD288 constructs yielded crystals either with an Avi tag sequence fused to the C-terminus (NBD288-Avi) or without an Avi tag (NBD288) diffracting to resolutions of 2.3 and 2.35 Å, respectively (Table 1). The NBD288-Avi crystals contained one molecule per asymmetric unit. Inspection of the NBD288-Avi crystal packing revealed an intriguing feature of the crystal lattice. The NBD288-Avi molecules are arranged as beads along the filament formed by protruding C-terminal Avi tags (Figure S6A−C of the Supporting Information). The Avi tag peptides form extended antiparallel β sheets that fit in the unoccupied ATP binding groove of a symmetry-related NBD288-Avi molecule. In the crystals formed by NBD288, three molecules that we call NBD288-chainA, NBD288-chainB, and NBD288-chainC were found in the asymmetric unit. In NBD288-chainA and NBD288-chainB, residues of the C-terminal 3C protease cleavage site, which remain fused to the protein after His tag cleavage, are structured and interact with residues of the NBD288 core, including the switch loop His548 (Figure S6D of the Supporting Information). In NBD288-chainC, however, the C-terminal cleavage artifact is unstructured. A closer inspection of the crystal contacts among the three NBD288 molecules of the asymmetric unit did not reveal functional NBD dimers (not shown). Superpositions of the Cα atoms of NBD288 with full-length apo TM287/288 (PDB entry 4Q4H) result in rmsds that range from a minimum of 1.16 Å for NBD288-chainC (over 234 residues) to a maximum of 1.53 Å for NBD288-Avi (over 236 residues). If not stated otherwise, our structural interpretation focuses on NBD288-chainC (Figure 5A), because this molecule is not influenced by the remains of the C-terminal 3C protease cleavage site. When the RecA-like domain of NBD288-chainC is superimposed on the full-length structure, a 5° rotation of the helical domain becomes apparent (Figure 3B).

The D-Loop of the Isolated NBD288 Is Flexible. Whereas all residues of NBD288-chainA could be built, NBD288-chainB, NBD288-chainC, and NBD288-Avi lack D-loop residues 520−522. Of note, the Cα atoms of residues 520−522 in NBD288-chainA exhibit a high average B factor of 116 Å^2 compared to an average B factor of 47 Å^2 for all Cα atoms of NBD288-chainA, indicating major flexibility in this region. In the full-length transporter, the D-loop of NBD2 establishes hydrogen bonds with NBD1 and provides a

DOI: 10.1021/acs.biochem.5b00188
Biochemistry 2015, 54, 3086−3099

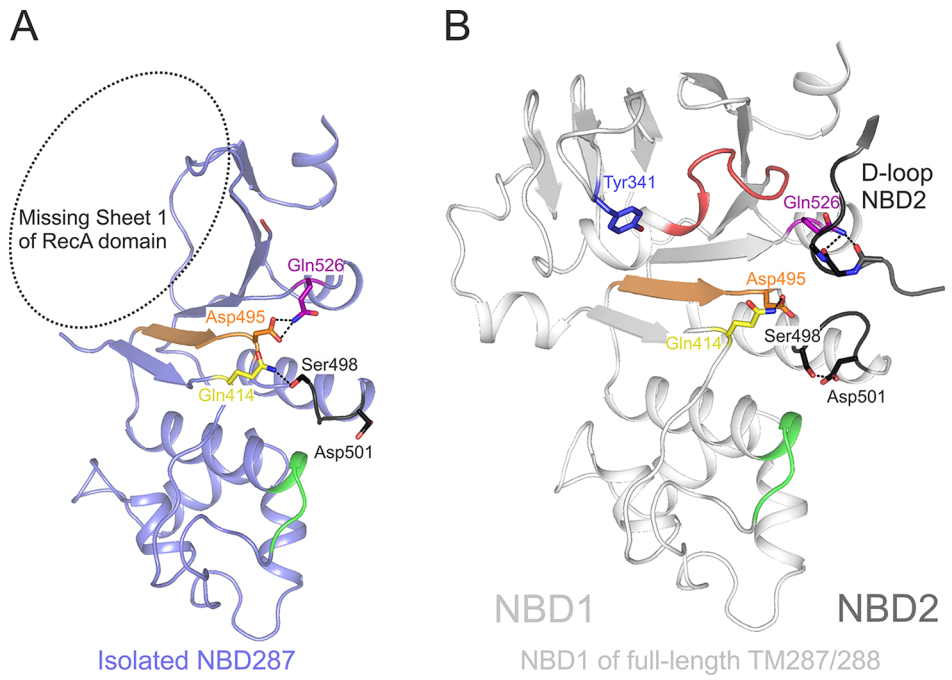

Figure 4. Structural analysis of NBD287. (A) Hydrogen bonds (cutoff of ≤3.6 Å) involving conserved residues are shown for the isolated NBD287 (blue). The color code depicting conserved motifs is identical to that used in Figure 2. Sheet 1 containing the A-loop and the Walker A motif is missing (dashed circle). (B) Hydrogen bonds of the same residues as in panel A are shown in the full-length apo TM287/288 context (colored light gray and dark gray). The D-loop of NBD2, which provides hydrogen bonding partners for key residues of NBD1, is shown.

significant interaction interface that keeps the NBDs together while the TMDs adopt an inward-oriented state (Figure 4B). Interestingly, we also observed a displacement of the helix following the D-loop, called the D-helix,[52] tilting along its long axis away from the RecA β-sheet by around 10° with respect to its position in the full-length transporter structure (Figure 3B). In HlyB, the D-helix (called helix 6 in that context) had been assigned the role of an enthalpic device, which is able to store energy gained from ATP hydrolysis in the form of elastic strain while the transporter converts from the ATP- to ADP-bound conformation to release ADP.[51] Our analysis of NBD288 rather suggests that D-loop flexibility and D-helix rotation play a role in interdomain communication as these structural elements interact with the Walker A motif of the neighboring NBD and thereby appear to be involved in the coordination of events taking place at the two ATPase sites.[30]

The Catalytic Dyad of the Consensus Site. Although NBD288 is capable of ATP binding (Figure 1D), we were not able to cocrystallize NBD288 with ATP or AMP-PNP. We also attempted to soak ATP and AMP-PNP into crystals obtained in the absence of nucleotides, which was not successful presumably because elements of the ATP binding site are involved in crystal contacts. In the AMP-PNP-bound structure of full-length TM287/288, only the degenerate site was occupied with a nucleotide, while nucleotide binding at the consensus site was not observed. However, it is generally accepted that the consensus site is chiefly responsible for ATP hydrolysis, and therefore, a nucleotide is expected to bind to this site to facilitate the transition to the outward-facing NBD-closed state. The Walker B glutamate (Glu517), which is acting as a catalytic base, and the switch loop histidine (His548) are of prime importance for ATP hydrolysis and consequently substrate transport. In contrast to HlyB, in which the switch loop H662A mutation but not the Walker B E631Q mutation fully abrogates ATPase activity,[43] we measured a higher residual activity for the H548A mutant [1.25 ± 0.15% of that of the wild type (wt)] than for the almost completely inactive E517Q mutant (0.20 ± 0.07% of that of the wt) in TM287/288 (Figure S7 of the Supporting Information). In the TM287/288 structure, Glu517 points its side chain away from the active site and is stabilized in its position via a hydrogen bond interaction with the highly conserved Gln498, which in turn is stabilized by a hydrogen bond with the ABC signature residue Gln494 (Figure 5B and Figure S8 of the Supporting Information). By contrast, in the solitary NBD288, the catalytic glutamate is pointing more toward the active site but still is locked by interactions with residues of the helix following the switch loop (Figure 5A). Such positioning of the catalytic base does not allow for polarization of the attacking water necessary for catalysis. The configuration of the catalytic residues is also shown in the context of the full-length exporter Sav1866 cocrystallized with AMP-PNP (Figure 5C).[53] In Sav1866, the Walker B glutamate is pointing toward the γ-phosphate and is assisted by an interaction with the switch loop histidine. An analogous pattern has also been observed for the maltose transporter cocrystallized in the presence of nucleotides.[10] Therefore, the consensus site of TM287/288 is thought to adopt a similar configuration during the transition from the inward- to outward-facing state to become catalytically active.

Interdomain Contacts between the NBDs and the Coupling Helices of the TMDs. In the full-length TM287/288 structure, sheet 1 of NBD1 forms half of the binding groove for intracellular loop 4 (ICL4) that protrudes from the TM288 polypeptide (Figure 6A). In addition, it also interacts with residues of ICL1. ICL1 and ICL4 contain the coupling helices, structural elements that transmit the motion of NBD closure to the reorientation of the transmembrane cavity.[7] Several residues of both coupling helices make direct contacts with sheet 1 (Figure 6B). Furthermore, the Walker A motif, which directly precedes sheet 1 (Figure 2), is interacting with

DOI: 10.1021/acs.biochem.5b00188
Biochemistry 2015, 54, 3086−3099

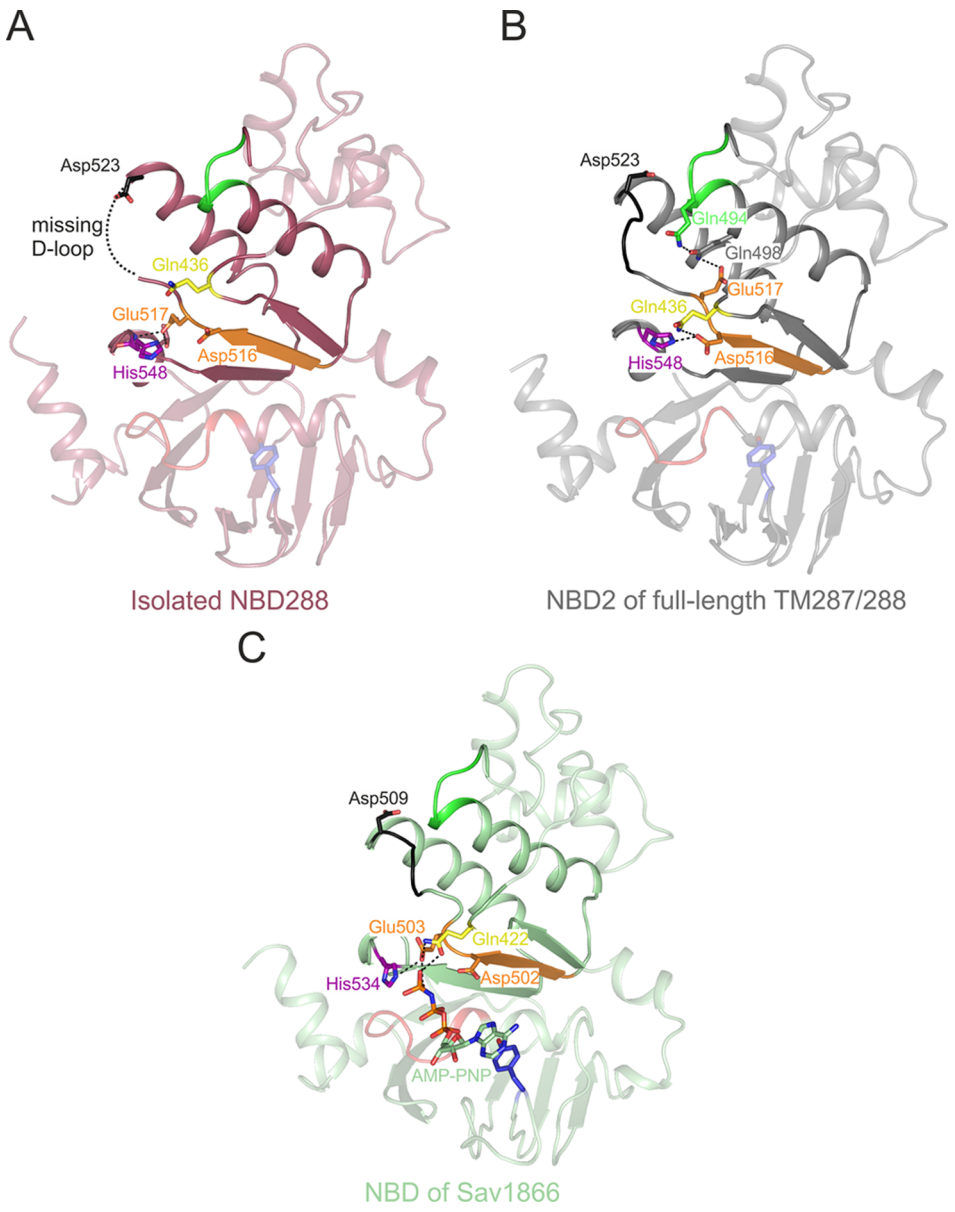

Figure 5. Structural analysis of NBD288. Hydrogen bonding pattern of key residues of the Walker B motif, the switch motif, the Q-loop, the D-loop, and the ABC signature motif are shown using the same color code as in Figure 2 for the isolated NBD288 (A), NBD2 embedded in apo TM287/288 (B), and Sav1866 (C). AMP-PNP bound in Sav1866 is depicted as sticks in panel C.

the D-loop and the D-helix of the neighboring NBD2 (Figure 4B). Therefore, lack of density for sheet 1 of NBD287 can be explained by the absence of the TM288 chain (its NBD and coupling helix), which provides important interaction residues likely facilitating its correct folding.

In NBD288, the corresponding binding groove accommodates the coupling helices of ICL2 and ICL3 of the transmembrane domains (Figure 6C); however, in contrast to NBD287, sheet 1 of NBD288 could be resolved. Upon docking of the coupling helices, the accommodating cleft surface changes its shape mainly because of modest side chain rearrangements. Notable exceptions are the residues following the Q-loop Gln436, which prominently shift toward and interact with ICL2 in full-length TM287/288 (Figure 6D). Once a nucleotide has bound to the consensus site during the transition to the outward-facing state, Gln436 is expected to interact with the γ-phosphate of ATP and thereby establishes a molecular communication pathway between the nucleotide binding site and the TMDs.

The Degenerate Site Forms Only in the Context of the Full-Length Transporter. When the partial structural models of NBD287 and NBD288 are oriented as they would face each other in the full-length protein, we see a striking correlation of the disordered areas with the location of the degenerate ATPase site (Figure 7). The missing parts of our models interact with other domains, namely the opposite NBD as well as with the coupling helix of ICL1 and ICL4 of the TMDs, in the full-length context. Importantly, these interdomain contacts are already established in apo TM287/288 (Figure 7B), and the degenerate site is arranged such that it can accommodate a nucleotide as seen in the TM287/288 structure with bound AMP-PNP (Figure 7C). The observed interdomain interactions are a prerequisite for binding of a nucleotide to the degenerate site, because binding of a nucleotide to the isolated NBD287 was not observed (Figure 1C). The interaction across domains

DOI: 10.1021/acs.biochem.5b00188
Biochemistry 2015, 54, 3086−3099

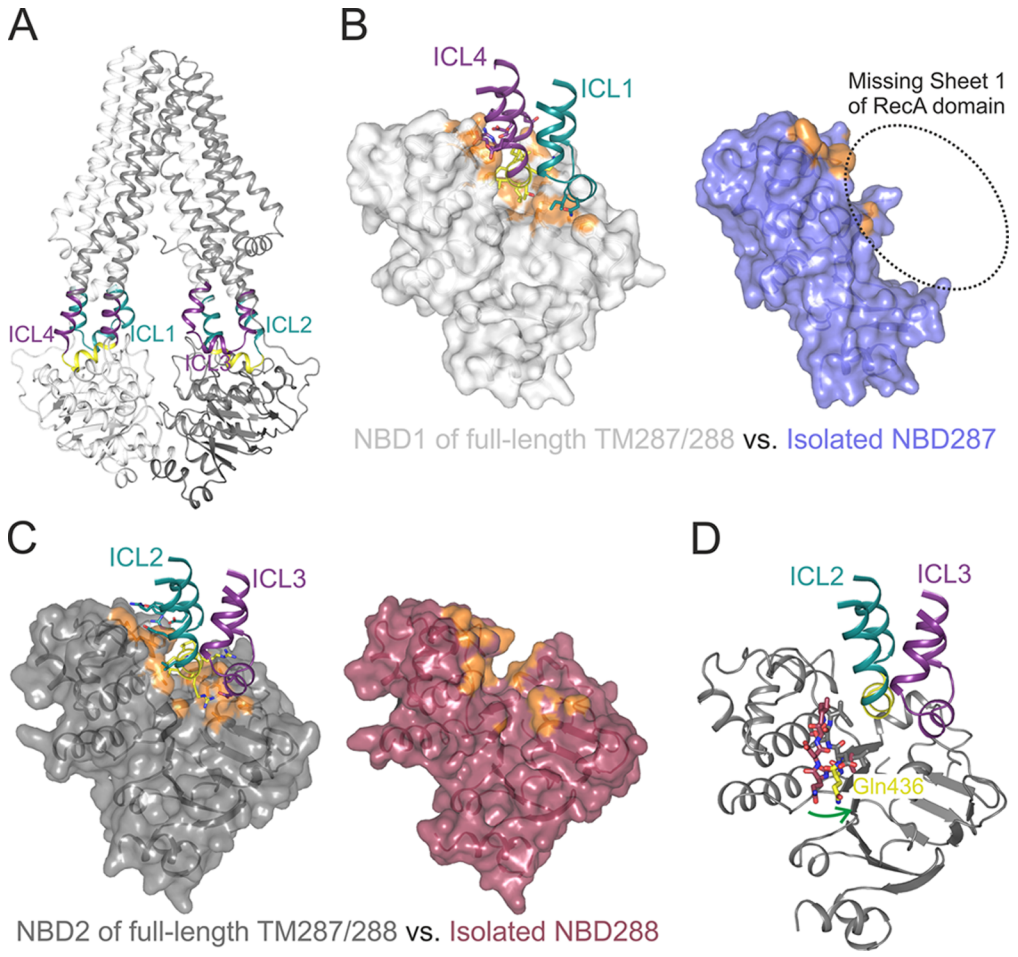

Figure 6. Binding of coupling helices into the NBD cleft. (A) Overview of apo TM287/288 with highlighted intracellular loops (ICL1−4) containing the coupling helices. TM287 is colored light gray and TM288 dark gray; the ICLs are colored deep teal and violet purple and the coupling helices of ICL2 and ICL4 yellow. (B) NBD1 (surface representation) interacting with ICL1 and ICL4 (shown as cartoons) in the full-length transporter complex (light gray, left) and isolated NBD287 (blue, right). NBD atoms interacting with the coupling helices are colored orange (distance cutoff for interactions of ≤4 Å). ICL residues contacting NBD1 are shown as sticks. (C) Analysis analogous to panel B for NBD2 interacting with ICL2 and ICL3. Context-embedded NBD2 is colored dark gray (left) and isolated NBD288 raspberry (right). (D) Movement of the Q-loop of NBD2 as a consequence of interaction with ICL2. The NBD-TMD interaction is shown for full-length TM287/288 (depicted as a cartoon with NBD2 colored dark gray). Residues following the Q-loop glutamine (Gln436, colored yellow) of TM287/288 are depicted as dark gray sticks. The corresponding Q-loop residues of the isolated NBD288 structure are shown as raspberry-colored sticks, and the Q-loop movement is emphasized by a green arrow.

also manifests in a temperature factor analysis. The temperature factor distribution along the isolated NBDs suggests that the area of the degenerate site is relatively more fexible than the region harboring the consensus site (Figure S9 of the Supporting Information). By contrast, in full-length apo TM287/288, the *B* factors are lowest in sheet 1 of the RecA-like domain of NBD1 and in the degenerate site in general. However, it needs to be mentioned that this region of NBD1 is involved in crystal contacts.

■ DISCUSSION

Currently, there are around 60 PDB entries describing the structures of isolated NBDs.[6] In the past 15 years, NBD structures greatly contributed to the understanding of ABC transporter function. First, they revealed today's generally accepted concept of ATP-induced dimerization of a pair of NBDs in its typical head-to-tail fashion, i.e., the so-called sandwich dimer.[23,24,35,43] Second, these high-resolution structures, in many cases of site-directed mutants, allowed for valuable insights into the molecular mechanism of ATP hydrolysis, which follows NBD dimerization. Third, analysis of the dimer interface revealed first insights into the cross-communication of the two ATP binding sites.[51]

As opposed to those of homodimeric NBD dimers, studies of isolated NBDs of heterodimeric ABC exporters appeared to be less straightforward. Well-studied examples are the NBDs of TAP1/2, MRP1, and CFTR, which by nature contain noncanonical substitutions at the catalytic dyad. For both NBDs of TAP1/2 and MRP1, nucleotide binding was reported.[28,54,55] Therefore, a lack of nucleotide binding by NBD287 appears to be a rather unique finding. Whereas the TAP1 NBD binds ADP stronger than ATP,[28] NBD288 binds only ATP, but not ADP. With regard to SEC analysis, nucleotide-induced dimer formation was reported for TAP1 NBD (rat homologue),[28] but neither for TAP2 NBD nor for the NBDs of MRP1.[55] Therefore, our observation that NBD287 and NBD288 did not dimerize in the presence of MgATP is in accord with the majority of previous reports. ATPase activities of isolated NBDs of TAP1/2 and MRP1 were reported to be very low[28,55] or absent,[54] which is in agreement

DOI: 10.1021/acs.biochem.5b00188
Biochemistry 2015, 54, 3086−3099

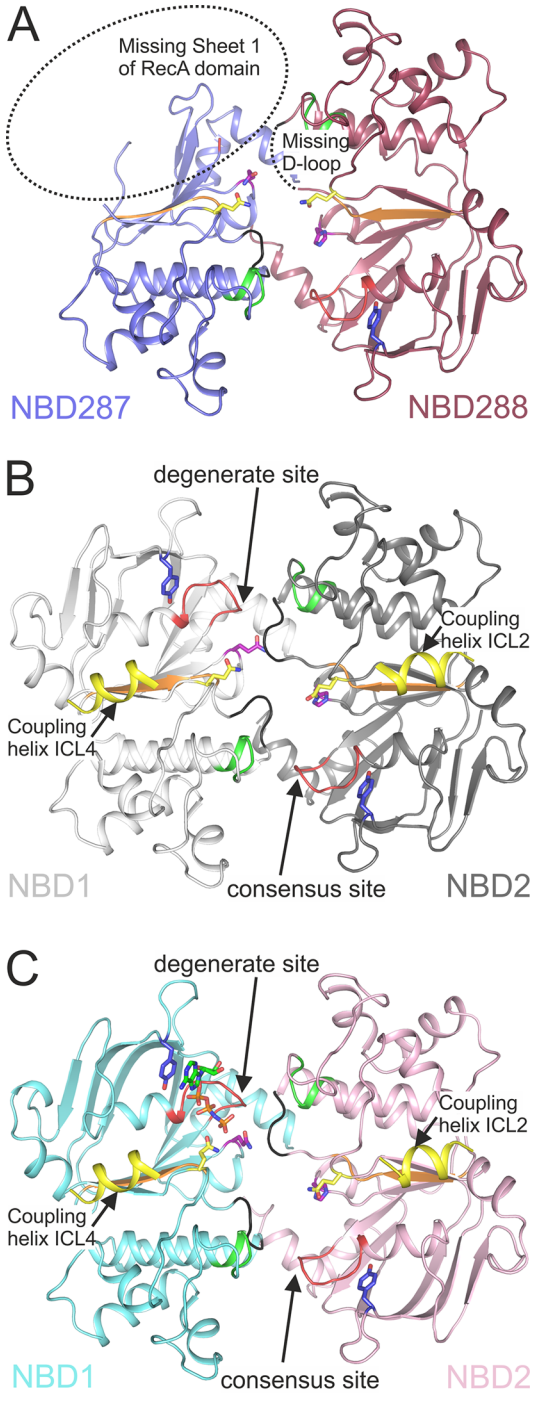

Figure 7. NBDs in the context of the full-length transporter. (A) NBD287 (blue) and NBD288 (raspberry) are positioned as they would face each other in full-length TM287/288. The missing parts are indicated by dashed lines. Conserved motifs are colored as indicated in Figure 2. (B) The heterodimeric assembly of NBD1 (light gray) and NBD2 (dark gray) is shown in the full-length context of apo TM287/288. The coupling helices of ICL2 and ICL4 are emphasized as yellow cartoons. (C) The same visualization as in panel B, but of the TM287/288 structure with AMP-PNP bound at the degenerate site (shown as sticks).

with our findings. Crystal structures of NBD1 of TAP1/2 (human homologue), MRP1, and CFTR depicted monomers, irrespective of whether nucleotides were included,[20,56,57] indicating that a NBD dimer containing two degenerate sites is not readily formed. Crystals of TAP1 NBD dimers (rat homologue) could be obtained by various combinations of mutations in the Walker B motif and the switch motif.[28] These structures permitted important insights into the structural arrangements of the degenerate site despite the fact that they represented artificial homodimeric assemblies. Structural representatives of the second NBD of heterodimeric ABC exporters, which contain the catalytic glutamate-histidine dyad, are scarce. The only published example is Py-MDR2, the second NBD of the presumed drug transporter MDR2 of the rodent parasite *Plasmodium yoelii*, which was crystallized by a structural genomics consortium.[58] Importantly, in spite of reported attempts with TAP1/2 and MRP1,[28,55] it turned out to be impossible to obtain a stable heterodimeric assembly of isolated NBDs. It was therefore the TM287/288 full-length structure that for the first time featured interactions between a heterodimeric NBD pair.[29]

This study permits an unprecedented comparison of the structures of a full-length ABC exporter with the isolated NBDs of the same protein. The isolated NBDs of TM287/288 are unable to hydrolyze ATP, and they neither homodimerize nor heterodimerize. This suggests that in TM287/288 a productive dimerization can take place only in the full-length protein. The isolated NBDs exhibit remarkable plasticity that appears to be necessary to support inter- and intrachain interactions in the full-length structure and conformational changes during the catalytic cycle. The RecA-like domain and the helical domain of both NBDs are able to rotate against each other as rigid bodies. This subdomain autonomy is necessary to accommodate the coupling helices of the transmembrane domains in a preformed cleft at the NBD surface. Docking of the coupling helices to the NBD groove can be seen as knob-into-hole binding. It is reminiscent to the maltose importer, the only other ABC transporter besides TM287/288 for which the structures of the isolated NBDs and the NBDs in the context of the fully assembled transporter have been described.[10,35] Previous studies of isolated NBDs of HlyB suggested that nucleotide binding governs the relative orientation between the RecA-like domain and the helical domain.[51] Their analysis revealed that ATP binding leads to an inward rotation of the helical domain. Our study suggests that the extensive interactions between the coupling helices and the NBDs influence the relative rotation between the two subdomains, as well, and result in an inward rotation of these two rigid bodies that is independent of nucleotide binding.

In the homodimeric ABC exporters LmrA and BmrA, the NBDs exhibit increased flexibility when the transporter is in its nucleotide-free resting state.[59,60] As opposed to TM287/288, the NBDs are expected to fully separate in apo LmrA and BmrA as seen in the structure of MsbA from *E. coli*.[9] Deuterium exchange experiments with BmrA suggested that the coupling helices even temporarily disengage from the NBDs under these conditions.[60] As observed in this study with NBD287 and NBD288 being more flexible as isolated proteins than in the context of the full-length transporter, a reduced number of interdomain contacts can explain increased NBD flexibility in the resting state of LmrA and BmrA.

Major elements that constitute the degenerate ATPase site could not be resolved in the isolated structures. The stability of sheet 1 of the RecA-like domain of NBD287 is compromised in the absence of the TM288 chain, and the D-loop of isolated NBD288 is flexible. In the full-length structure of TM287/288, exactly these flexible portions interact with each other and in

DOI: 10.1021/acs.biochem.5b00188
Biochemistry 2015, 54, 3086−3099

addition appear to require the interaction with the coupling helix of ICL4 to become structured. Notably, the addition of nucleotides to NBD287 alone or mixed with NBD288 was not sufficient to stabilize the degenerate site, because neither dimer formation nor ATP hydrolysis was observed. Rather, the degenerate site needs to be preformed in the context of the full-length transporter to accommodate nucleotides.

The D-loop and Q-loop have been suggested to mediate molecular communication between subdomains of ABC transporters.[7,11,27,30,51,52,61] Interestingly, the most prominent differences between isolated NBD288 and the domain embedded in full-length TM287/288 are precisely observed in these two regions. In the intact transporter, the D-loop and the D-helix of NBD2 establish extensive contacts with NBD1 and the Q-loop interacts with the coupling helix of ICL2 of TM287. The areas that build the composite canonical ATPase site (the Walker A motif, the Walker B motif, and the H-loop of NBD2 and the D-loop and the ABC signature of NBD1) are structured in the isolated NBDs. However, Glu517 and His548 constituting the catalytic dyad of the consensus site undergo major conformational changes once they are in the context of the full-length protein. This illustrates that structural details concerning functionally important residues in isolated NBDs should be interpreted with great care. As it turns out, conserved residues of the Walker B motif, the switch loop, the Q-loop, and the D-loop of both NBDs exhibit completely different hydrogen bonding patterns in isolation and in the multidomain transporter complex. This is probably not further surprising; these key residues are strategically positioned at the NBD surface in such a manner that they can change their interaction partner during the transport cycle. The real bonding partners can thus only be determined in the context of the full-length transporter, because many of the key residues in ABC transporters, in particular those involved in interdomain communication, interact across domains.

In summary, our analysis reveals that the motor domains of TM287/288 become fully structured only in the heterodimeric arrangement of the intact transporter. In particular, the formation of the composite degenerate site is critically dependent on interdomain contacts that keep the NBDs together when the transporter adopts its inward-facing state even in the absence of nucleotides. More generally, this study illustrates that a multidomain transporter complex is more than the sum of its individual parts.

■ ASSOCIATED CONTENT

Supporting Information

Production levels and purification of NBD287 and NBD288 expressed from the various tested constructs are summarized in Table S1. Further SEC profiles are shown in Figure S1. The original data of SYPRO unfolding are shown in Figure S2. Structural analysis of the amphipatic helix of sheet 1 interacting with sheet 2 of NBD287 is shown in Figure S3. An analysis of dissolved NBD287 crystals is shown in Figure S4. Figures S5 and S8 show electron densities for conserved residues of NBD287 and NBD288, respectively. Figure S6 features a structural analysis of NBD288 and NBD288-Avi. Figure S7 shows ATPase activities of the E517Q and H548A mutants of TM287/288. A temperature factor analysis of isolated NBDs versus full-length apo TM287/288 is shown in Figure S9. The Supporting Information is available free of charge on the ACS Publications website at DOI: 10.1021/acs.biochem.5b00188.

Accession Codes

The crystal structures were deposited in the PDB as entries 4Q7K (NBD287), 4Q7L (NBD288), and 4Q7M (NBD288-Avi).

■ AUTHOR INFORMATION

Corresponding Authors

*E-mail: m.seeger@imm.uzh.ch.
*E-mail: gruetter@bioc.uzh.ch.

Present Address

§E.R.G.: Institute of Biochemistry, Biocenter, Goethe-University Frankfurt, Max-von-Laue-Str. 9, D-60438 Frankfurt am Main, Germany.

Author Contributions

M.A.B. and M.H. contributed equally to this work.

Funding

This work was supported by the Swiss National Center of Competence in Research (NCCR) Structural Biology (to M.G.G.), an Ambizione grant and an SNF Professorship of the Swiss National Science Foundation (both to M.A.S.), and a postdoctoral fellowship from the Human Frontier Science Program (to E.R.G.).

Notes

The authors declare no competing financial interest.

■ ACKNOWLEDGMENTS

We thank Dr. Hüseyin Besir from the Protein Expression & Purification Core Facility at the EMBL Heidelberg for providing us the pETM11-SUMO3GFP construct and an expression vector for the SenP2 protease. We acknowledge Beat Blattmann and Céline Stutz-Ducommun of the Protein Crystallization Center UZH for performing the crystallization screening, Dr. Christophe Briand and the SLS X06SA beamline staff for their assistance in diffraction data collection, Dr. Iwan Zimmermann for his help in conducting unfolding experiments with SYPRO Orange, and Dr. Serge Chesnov from FGCZ for mass spectrometry analysis of the NBD287 crystals.

■ REFERENCES

(1) Davidson, A. L., Dassa, E., Orelle, C., and Chen, J. (2008) Structure, function, and evolution of bacterial ATP-binding cassette systems. *Microbiol. Mol. Biol. Rev. 72*, 317−364.

(2) Riordan, J. R., Rommens, J. M., Kerem, B. S., Alon, N., Rozmahel, R., Grzelczak, Z., Zielenski, J., Lok, S., Plavsic, N., Chou, J. L., Drumm, M. L., Iannuzzi, M. C., Collins, F. S., and Tsui, L. C. (1989) Identification of the Cystic-Fibrosis Gene: Cloning and Characterization of Complementary-DNA. *Science 245*, 1066−1072.

(3) Allikmets, R., Shroyer, N. F., Singh, N., Seddon, J. M., Lewis, R. A., Bernstein, P. S., Peiffer, A., Zabriskie, N. A., Li, Y., Hutchinson, A., Dean, M., Lupski, J. R., and Leppert, M. (1997) Mutation of the Stargardt disease gene (ABCR) in age-related macular degeneration. *Science 277*, 1805−1807.

(4) Mosser, J., Lutz, Y., Stoeckel, M. E., Sarde, C. O., Kretz, C., Douar, A. M., Lopez, J., Aubourg, P., and Mandel, J. L. (1994) The Gene Responsible for Adrenoleukodystrophy Encodes a Peroxisomal Membrane-Protein. *Hum. Mol. Genet. 3*, 265−271.

(5) Gottesman, M. M., and Ling, V. (2006) The molecular basis of multidrug resistance in cancer: The early years of P-glycoprotein research. *FEBS Lett. 580*, 998−1009.

(6) Haffke, M., Menzel, A., Carius, Y., Jahn, D., and Heinz, D. W. (2010) Structures of the nucleotide-binding domain of the human ABCB6 transporter and its complexes with nucleotides. *Acta Crystallogr. D66*, 979−987.

DOI: 10.1021/acs.biochem.5b00188
Biochemistry 2015, 54, 3086−3099

(7) Dawson, R. J., and Locher, K. P. (2006) Structure of a bacterial multidrug ABC transporter. *Nature 443*, 180−185.
(8) Aller, S. G., Yu, J., Ward, A., Weng, Y., Chittaboina, S., Zhuo, R., Harrell, P. M., Trinh, Y. T., Zhang, Q., Urbatsch, I. L., and Chang, G. (2009) Structure of P-glycoprotein reveals a molecular basis for poly-specific drug binding. *Science 323*, 1718−1722.
(9) Ward, A., Reyes, C. L., Yu, J., Roth, C. B., and Chang, G. (2007) Flexibility in the ABC transporter MsbA: Alternating access with a twist. *Proc. Natl. Acad. Sci. U.S.A. 104*, 19005−19010.
(10) Oldham, M. L., Khare, D., Quiocho, F. A., Davidson, A. L., and Chen, J. (2007) Crystal structure of a catalytic intermediate of the maltose transporter. *Nature 450*, 515−521.
(11) Locher, K. P., Lee, A. T., and Rees, D. C. (2002) The *E. coli* BtuCD structure: A framework for ABC transporter architecture and mechanism. *Science 296*, 1091−1098.
(12) Hollenstein, K., Frei, D. C., and Locher, K. P. (2007) Structure of an ABC transporter in complex with its binding protein. *Nature 446*, 213−216.
(13) Gerber, S., Comellas-Bigler, M., Goetz, B. A., and Locher, K. P. (2008) Structural basis of trans-inhibition in a molybdate/tungstate ABC transporter. *Science 321*, 246−250.
(14) Pinkett, H. W., Lee, A. T., Lum, P., Locher, K. P., and Rees, D. C. (2007) An inward-facing conformation of a putative metal-chelate-type ABC transporter. *Science 315*, 373−377.
(15) Jin, M. S., Oldham, M. L., Zhang, Q., and Chen, J. (2012) Crystal structure of the multidrug transporter P-glycoprotein from *Caenorhabditis elegans*. *Nature 490*, 566−569.
(16) Lee, J. Y., Yang, J. G., Zhitnitsky, D., Lewinson, O., and Rees, D. C. (2014) Structural Basis for Heavy Metal Detoxification by an Atm1-Type ABC Exporter. *Science 343*, 1133−1136.
(17) Srinivasan, V., Pierik, A. J., and Lill, R. (2014) Crystal Structures of Nucleotide-Free and Glutathione-Bound Mitochondrial ABC Transporter Atm1. *Science 343*, 1137−1140.
(18) Kodan, A., Yamaguchi, T., Nakatsu, T., Sakiyama, K., Hipolito, C. J., Fujioka, A., Hirokane, R., Ikeguchi, K., Watanabe, B., Hiratake, J., Kimura, Y., Suga, H., Ueda, K., and Kato, H. (2014) Structural basis for gating mechanisms of a eukaryotic P-glycoprotein homolog. *Proc. Natl. Acad. Sci. U.S.A. 111*, 4049−4054.
(19) Choudhury, H. G., Tong, Z., Mathavan, I., Li, Y. Y., Iwata, S., Zirah, S., Rebuffat, S., van Veen, H. W., and Beis, K. (2014) Structure of an antibacterial peptide ATP-binding cassette transporter in a novel outward occluded state. *Proc. Natl. Acad. Sci. U.S.A. 111*, 9145−9150.
(20) Gaudet, R., and Wiley, D. C. (2001) Structure of the ABC ATPase domain of human TAP1, the transporter associated with antigen processing. *EMBO J. 20*, 4964−4972.
(21) Schmitt, L., Benabdelhak, H., Blight, M. A., Holland, I. B., and Stubbs, M. T. (2003) Crystal structure of the nucleotide-binding domain of the ABC-transporter haemolysin B: Identification of a variable region within ABC helical domains. *J. Mol. Biol. 330*, 333−342.
(22) Jones, P. M., and George, A. M. (1999) Subunit interactions in ABC transporters: Towards a functional architecture. *FEMS Microbiol. Lett. 179*, 187−202.
(23) Hopfner, K. P., Karcher, A., Shin, D. S., Craig, L., Arthur, L. M., Carney, J. P., and Tainer, J. A. (2000) Structural biology of Rad50 ATPase: ATP-driven conformational control in DNA double-strand break repair and the ABC-ATPase superfamily. *Cell 101*, 789−800.
(24) Smith, P. C., Karpowich, N., Millen, L., Moody, J. E., Rosen, J., Thomas, P. J., and Hunt, J. F. (2002) ATP binding to the motor domain from an ABC transporter drives formation of a nucleotide sandwich dimer. *Mol. Cell 10*, 139−149.
(25) Aittoniemi, J., Fotinou, C., Craig, T. J., de Wet, H., Proks, P., and Ashcroft, F. M. (2009) SUR1: A unique ATP-binding cassette protein that functions as an ion channel regulator. *Philos. Trans. R. Soc., B 364*, 257−267.
(26) Csanady, L., Mihalyi, C., Szollosi, A., Torocsik, B., and Vergani, P. (2013) Conformational changes in the catalytically inactive nucleotide-binding site of CFTR. *J. Gen. Physiol. 142*, 61−73.
(27) Grossmann, N., Vakkasoglu, A. S., Hulpke, S., Abele, R., Gaudet, R., and Tampe, R. (2014) Mechanistic determinants of the directionality and energetics of active export by a heterodimeric ABC transporter. *Nat. Commun. 5*, 5419.
(28) Procko, E., Ferrin-O'Connell, I., Ng, S. L., and Gaudet, R. (2006) Distinct structural and functional properties of the ATPase sites in an asymmetric ABC transporter. *Mol. Cell 24*, 51−62.
(29) Hohl, M., Briand, C., Grütter, M. G., and Seeger, M. A. (2012) Crystal structure of a heterodimeric ABC transporter in its inward-facing conformation. *Nat. Struct. Mol. Biol. 19*, 395−402.
(30) Hohl, M., Hürlimann, L. M., Böhm, S., Schöppe, J., Grütter, M. G., Bordignon, E., and Seeger, M. A. (2014) Structural basis for allosteric cross-talk between the asymmetric nucleotide binding sites of a heterodimeric ABC exporter. *Proc. Natl. Acad. Sci. U.S.A. 111*, 11025−11030.
(31) Shintre, C. A., Pike, A. C., Li, Q., Kim, J. I., Barr, A. J., Goubin, S., Shrestha, L., Yang, J., Berridge, G., Ross, J., Stansfeld, P. J., Sansom, M. S., Edwards, A. M., Bountra, C., Marsden, B. D., von Delft, F., Bullock, A. N., Gileadi, O., Burgess-Brown, N. A., and Carpenter, E. P. (2013) Structures of ABCB10, a human ATP-binding cassette transporter in apo- and nucleotide-bound states. *Proc. Natl. Acad. Sci. U.S.A. 110*, 9710−9715.
(32) Mittal, A., Böhm, S., Grütter, M. G., Bordignon, E., and Seeger, M. A. (2012) Asymmetry in the homodimeric ABC transporter MsbA recognized by a DARPin. *J. Biol. Chem. 287*, 20395−20406.
(33) Borbat, P. P., Surendhran, K., Bortolus, M., Zou, P., Freed, J. H., and McHaourab, H. S. (2007) Conformational motion of the ABC transporter MsbA induced by ATP hydrolysis. *PLoS Biol. 5*, e271.
(34) Verhalen, B., and Wilkens, S. (2011) P-glycoprotein Retains Drug-stimulated ATPase Activity upon Covalent Linkage of the Two Nucleotide Binding Domains at Their C-terminal Ends. *J. Biol. Chem. 286*, 10476−10482.
(35) Chen, J., Lu, G., Lin, J., Davidson, A. L., and Quiocho, F. A. (2003) A tweezers-like motion of the ATP-binding cassette dimer in an ABC transport cycle. *Mol. Cell 12*, 651−661.
(36) Geertsma, E. R., and Dutzler, R. (2011) A versatile and efficient high-throughput cloning tool for structural biology. *Biochemistry 50*, 3272−3278.
(37) Hartley, J. L., Temple, G. F., and Brasch, M. A. (2000) DNA cloning using in vitro site-specific recombination. *Genome Res. 10*, 1788−1795.
(38) Costa, S. J., Almeida, A., Castro, A., Domingues, L., and Besir, H. (2013) The novel Fh8 and H fusion partners for soluble protein expression in *Escherichia coli*: A comparison with the traditional gene fusion technology. *Appl. Microbiol. Biotechnol. 97*, 6779−6791.
(39) Kabsch, W. (2010) XDS. *Acta Crystallogr. D66*, 125−132.
(40) McCoy, A. J., Grosse-Kunstleve, R. W., Adams, P. D., Winn, M. D., Storoni, L. C., and Read, R. J. (2007) Phaser crystallographic software. *J. Appl. Crystallogr. 40*, 658−674.
(41) Emsley, P., Lohkamp, B., Scott, W. G., and Cowtan, K. (2010) Features and development of Coot. *Acta Crystallogr. D66*, 486−501.
(42) Adams, P. D., Afonine, P. V., Bunkoczi, G., Chen, V. B., Davis, I. W., Echols, N., Headd, J. J., Hung, L. W., Kapral, G. J., Grosse-Kunstleve, R. W., McCoy, A. J., Moriarty, N. W., Oeffner, R., Read, R. J., Richardson, D. C., Richardson, J. S., Terwilliger, T. C., and Zwart, P. H. (2010) PHENIX: A comprehensive Python-based system for macromolecular structure solution. *Acta Crystallogr. D66*, 213−221.
(43) Zaitseva, J., Jenewein, S., Jumpertz, T., Holland, I. B., and Schmitt, L. (2005) H662 is the linchpin of ATP hydrolysis in the nucleotide-binding domain of the ABC transporter HlyB. *EMBO J. 24*, 1901−1910.
(44) Moody, J. E., Millen, L., Binns, D., Hunt, J. F., and Thomas, P. J. (2002) Cooperative, ATP-dependent association of the nucleotide binding cassettes during the catalytic cycle of ATP-binding cassette transporters. *J. Biol. Chem. 277*, 21111−21114.
(45) Syberg, F., Suveyzdis, Y., Kotting, C., Gerwert, K., and Hofmann, E. (2012) Time-resolved Fourier transform infrared spectroscopy of the nucleotide-binding domain from the ATP-binding cassette transporter MsbA: ATP hydrolysis is the rate-limiting step in the catalytic cycle. *J. Biol. Chem. 287*, 23923−23931.

DOI: 10.1021/acs.biochem.5b00188
Biochemistry 2015, 54, 3086−3099

(46) Orelle, C., Gubellini, F., Durand, A., Marco, S., Levy, D., Gros, P., Di Pietro, A., and Jault, J. M. (2008) Conformational change induced by ATP binding in the multidrug ATP-binding cassette transporter BmrA. *Biochemistry 47*, 2404−2412.
(47) Kim, I. W., Peng, X. H., Sauna, Z. E., FitzGerald, P. C., Xia, D., Muller, M., Nandigama, K., and Ambudkar, S. V. (2006) The conserved tyrosine residues 401 and 1044 in ATP sites of human P-glycoprotein are critical for ATP binding and hydrolysis: Evidence for a conserved subdomain, the A-loop in the ATP-binding cassette. *Biochemistry 45*, 7605−7616.
(48) Ericsson, U. B., Hallberg, B. M., Detitta, G. T., Dekker, N., and Nordlund, P. (2006) Thermofluor-based high-throughput stability optimization of proteins for structural studies. *Anal. Biochem. 357*, 289−298.
(49) Karpowich, N., Martsinkevich, O., Millen, L., Yuan, Y. R., Dai, P. L., MacVey, K., Thomas, P. J., and Hunt, J. F. (2001) Crystal structures of the MJ1267 ATP binding cassette reveal an induced-fit effect at the ATPase active site of an ABC transporter. *Structure 9*, 571−586.
(50) Zaitseva, J., Jenewein, S., Wiedenmann, A., Benabdelhak, H., Holland, I. B., and Schmitt, L. (2005) Functional characterization and ATP-induced dimerization of the isolated ABC-domain of the haemolysin B transporter. *Biochemistry 44*, 9680−9690.
(51) Zaitseva, J., Oswald, C., Jumpertz, T., Jenewein, S., Wiedenmann, A., Holland, I. B., and Schmitt, L. (2006) A structural analysis of asymmetry required for catalytic activity of an ABC-ATPase domain dimer. *EMBO J. 25*, 3432−3443.
(52) Jones, P. M., and George, A. M. (2012) Role of the D-loops in allosteric control of ATP hydrolysis in an ABC transporter. *J. Phys. Chem. A 116*, 3004−3013.
(53) Dawson, R. J., and Locher, K. P. (2007) Structure of the multidrug ABC transporter Sav1866 from *Staphylococcus aureus* in complex with AMP-PNP. *FEBS Lett. 581*, 935−938.
(54) Ernst, R., Koch, J., Horn, C., Tampe, R., and Schmitt, L. (2006) Engineering ATPase activity in the isolated ABC cassette of human TAP1. *J. Biol. Chem. 281*, 27471−27480.
(55) Ramaen, O., Sizun, C., Pamlard, O., Jacquet, E., and Lallemand, J. Y. (2005) Attempts to characterize the NBD heterodimer of MRP1: Transient complex formation involves Gly771 of the ABC signature sequence but does not enhance the intrinsic ATPase activity. *Biochem. J. 391*, 481−490.
(56) Ramaen, O., Leulliot, N., Sizun, C., Ulryck, N., Pamlard, O., Lallemand, J. Y., Tilbeurgh, H., and Jacquet, E. (2006) Structure of the human multidrug resistance protein 1 nucleotide binding domain 1 bound to Mg^{2+}/ATP reveals a non-productive catalytic site. *J. Mol. Biol. 359*, 940−949.
(57) Lewis, H. A., Buchanan, S. G., Burley, S. K., Conners, K., Dickey, M., Dorwart, M., Fowler, R., Gao, X., Guggino, W. B., Hendrickson, W. A., Hunt, J. F., Kearins, M. C., Lorimer, D., Maloney, P. C., Post, K. W., Rajashankar, K. R., Rutter, M. E., Sauder, J. M., Shriver, S., Thibodeau, P. H., Thomas, P. J., Zhang, M., Zhao, X., and Emtage, S. (2004) Structure of nucleotide-binding domain 1 of the cystic fibrosis transmembrane conductance regulator. *EMBO J. 23*, 282−293.
(58) Vedadi, M., Lew, J., Artz, J., Amani, M., Zhao, Y., Dong, A., Wasney, G. A., Gao, M., Hills, T., Brokx, S., Qiu, W., Sharma, S., Diassiti, A., Alam, Z., Melone, M., Mulichak, A., Wernimont, A., Bray, J., Loppnau, P., Plotnikova, O., Newberry, K., Sundararajan, E., Houston, S., Walker, J., Tempel, W., Bochkarev, A., Kozieradzki, I., Edwards, A., Arrowsmith, C., Roos, D., Kain, K., and Hui, R. (2007) Genome-scale protein expression and structural biology of *Plasmodium falciparum* and related Apicomplexan organisms. *Mol. Biochem. Parasitol. 151*, 100−110.
(59) Siarheyeva, A., Lopez, J. J., Lehner, I., Hellmich, U. A., van Veen, H. W., and Glaubitz, C. (2007) Probing the molecular dynamics of the ABC multidrug transporter LmrA by deuterium solid-state nuclear magnetic resonance. *Biochemistry 46*, 3075−3083.
(60) Mehmood, S., Domene, C., Forest, E., and Jault, J. M. (2012) Dynamics of a bacterial multidrug ABC transporter in the inward- and outward-facing conformations. *Proc. Natl. Acad. Sci. U.S.A. 109*, 10832−10836.
(61) Urbatsch, I. L., Gimi, K., Wilke-Mounts, S., and Senior, A. E. (2000) Investigation of the role of glutamine-471 and glutamine-1114 in the two catalytic sites of P-glycoprotein. *Biochemistry 39*, 11921−11927.

DOI: 10.1021/acs.biochem.5b00188
Biochemistry 2015, 54, 3086−3099